DRUG DEVELOPMENT AND INDUSTRIAL PHARMACY, 4(1), 69-94 (1978)

MEASUREMENT OF INTERPARTICLE VOIDAGE AND PARTICLE CONTACT AREA IN COMPACTS BY NITROGEN ADSORPTION

N. G. Stanley-Wood and M. E. Johansson
Postgraduate school of Studies in Powder Technology
University of Bradford
Bradford, West Yorkshire, BD7, 1DP, England

1. INTRODUCTION

The mechanisms of powder compaction have been described as being due to either the plastic deformation or the fragmentation of individual particles with subsequent particle-particle bond formation (7, 8, 15, 18).

Many relationships between the physical properties of a powder, such as particle size, shape, size distribution and the packing of particles, have been proposed to predict the degree of densification. As a result an enormous number of mathematical relationships have been formulated between the pressure of compaction and the volume reduction of powders undergoing compaction (2, 10, 14, 21). Little information however is available on either the surface area and voidage of compacts or the fundamental parameter of contact area between particles at various degrees of compaction.

In a fundamental study of compressible powders, Shapiro (19) showed that the load bearing surface or particle contact area of plastically deforming magnesium spheres increased with increase in axially applied compaction force. This type of plastic material produced a linear relationship between the logarithmic porosity and

the compaction pressure. With thoria powder a non-linear relationship between the logarithmic porosity and the compaction pressure. With thoria powder a non-linear relationship between the logarithmic porosity versus compaction pressure was found. The non-linear relationship was found to be due to the fragmentation of the thoria particles and the movement of these small particles away from the load bearing surfaces.

Measurement of solely the surface area of powders under different degrees of compaction has shown conflicting results. In some cases the surface area with increase in compaction pressure whilst other compacts have shown a decrease in surface area (1, 7, 9, 11 and 12). Measurement of the variation of surface area with increase in compaction pressure with different types of material, such as a plastic (sodium chloride) or a brittle (sucrose) or an intermediate (coal) material, was attempted by Hardman and Lilley (9). The surface area of compacted and uncompacted powders was evaluated by the measurement of the amount of nitrogen gas adsorbed onto a solid at liquid nitrogen temperature. No attempt was made however to characterize the porous nature of the material before and after compaction, nor was any attempt made to calculate the interparticle voidage within the compact.

From nitrogen adsorption isotherms it is possible to calculate the surface area of powders and powder compacts from the well known Brunauer, Emmett and Teller (B.E.T.) equation (5). In addition the porous nature and pore size distribution in a material can also be qualitatively determined from the same isotherm by application of the Kelvin equation. Although the Kelvin equation was the original equation used to give an approximate pore size distribution in solid material or solid compacts, more sophisticated mathematical pore

models are now available for the determination of pore size. These models regard the pores within a solid as in the form of either a circular capillary (3, 6 and 16) or a parallel plate (13, 17).

The models also consider the effect of the build-up of multilayers of adsorbed molecules on the curved surfaces and the subsequent liquid condensation of adsorbed phase within pores.

Barrett Joyner and Halenda (B.J.H.) (3) derived from the Kelvin equation an equation which, from the volume of nitrogen gas desorbed at specific relative pressures, evaluated the true size of a pore (r_p) rather than the smaller Kelvin pore size (r_K). The difference between the Kelvin pore radius and the pore radius occurred because of the build-up of layers of adsorbed molecules on the surface of the solid and on the curved surfaces of the pore walls. The thickness of the adsorbed layer is not a simple linear relationship with relative pressure as aon a flat solid surface, but a relationship which varies with the size of the pore.

The degree of curvature of a cylindrical pore increases as the radial dimension of the pore becomes smaller and smaller. The thickness of the adsorbed layers in the pore are therefore a function of the pore size. A correction term, C, to compensate for a filled pore, a partially filled pore and an empty pore is incorporated into the B.J.H. model. The correction term is limited however to pores of less than 300 Å (30.0 nm) diameter. The same correction term is applicable to the area of a partially covered pore and the area of an empty pore. The B.J.H. equation was originally derived for the analysis of the desorption curve of an adsorption curve of an adsorption isotherm in negative pres-

sure increments. Later Cranston and Inkley (C.I.) of pore sizes by deriving a similar equation to B.J.H. and the C.I. equations can be applied to either the adsorption or desorption branch of an adsorption isotherm is used in preference to the desorption branch of an adsorption isotherm is used in preference to the desorption branch for pore size determinations (6, 16 and 17).

The strength of a bond between two solids is due to the area over which they are in contact. The contact area between particles, especially for plastic materials, can be taken as equivalent to half the difference between the surface area of particles before and after compaction. Contact area derived from surface areas measured by nitrogen adsorption will only be an approximation because errors will arise from the roughness of the particle surfaces and the inability of the nitrogen molecule, at liquid nitrogen temperatures, to penetrate openings smaller than two nanometers.

In this work three different directly compressible materials were taken and the surface areas and intraparticle porosities of the compacted and uncompacted particles were determined by nitrogen adsorption at a temperature of 77 K. From the adsorption isotherm obtained from each compacted material an interparticle voidage and a contact area between particles was calculated.

2. EXPERIMENTAL

2.1 Powders

2.1.1. Magnesium oxide

This is a calcined magnesium hydroxide (MgO) as supplied by Steetly (Mfg.) Ltd., Magnesia Division, Hartlepool. The mean particle size is 5.2 micrometre

as determined by an air pycnometer (Beckman Model 930) was 3.05 x 10^3 kg m^{-3}. 2.1.2 Bentonite.

This is a colloidal hydrated aluminum silicate consisting mainly of montmorillonite (Al_2O_3,$4SiO_2H_2O$) supplied by Reynolds and Branson Ltd., Leeds. The mean particle size by scanning photosedimentation is 22.0 micrometre and the density, by air pycnometry is is 2.71 x 10^3 kg m^{-3}.

2.1.3 Magnesium trisilicate

This is a hydrated magnesium silicate (2 MgO, 3 SiO_2) supplied by Reynolds and Branson Ltd., Leeds. The mean particle size by scanning photosedimentation is 15.1 micrometre and the density is 2.20 x 10^3 x 10^3 kg m^{-3} by air pycnometry.

2.2 Compacts

Each compact was individually prepared by placing approximately one gram of powder into a lubricated 1.27 cm internal diameter stainless steel die. The die and punches were lubricated with a 0.1% by weight solution of magnesium stearate in acetone prior to each compaction. The die was then left for 5 minutes for the acetone to evaporate from the die surfaces. The lower punch and die assembly were mounted on a movable lower platen of an Apex hydraulic press. Compaction occurred uniaxially by raising the lower platen containing the powder filled die, to the upper fixed platen containing the upper punch. The uniaxial compaction force applied to the powder was measured by a pound force pressure guage connected to the base of the hydraulic press. Ejection of the compact, from the die, was achieved by separation of the two halves of the die. The maximum force on the compact was therefore always in the compact mode. All compacts were prepared in a relative humidity of 25% in a temperature controlled (23.0^{o}C) room.

2.3 Adsorption Iso therms

Adsorption isotherms of compacted and uncompacted powders were obtained by low temperature nitrogen adsorption . The apparatus used is similar to that described in British Standard 4359 (4) except that the mercury manometer, which records the adsorption pressure, had been extended so that pressures in excess of one atmosphere (101 kPa) could be measured.

All the uncompacted and compacted powder samples were degassed, prior to nitrogen adsorption, at room temperature ($23.0^{\circ}C \pm 1^{\circ}C$) for 16 hours. The temperature of adsorption was at 77 K and the nitrogen gas used was research grade XX from B.O.C., Deer Park, Wembley. The adsorption sample when the adsorption isotherms on compacts was measured contained at least three compacts compacted at an identical compaction pressure. The surface area was calculated from the B.E.T. equation over the relative pressure range 0.05 to 0.35 and the pore size distribution and intraparticle porosity calculated from a FORTRAN computer program of the modified mathematical porous model of Barrett, Joyner and Haldena.

2.4 Computer Program

From the adsorption isotherm, a graph of relative pressure versus volume adsorbed per gram of solid, 40 values of the amount of nitrogen adsorbed into or onto the solid surface at specific relative pressure were taken. The relative pressure values were taken in known positive incremental steps and these, together with the appropriate volumes adsorbed per gram of sample were the input data to the computer. The computer program was written in FORTRAN for use on an I.C.L. (1904) computer. The FORTRAN program for the calculation of Kelvin's radius, statistical thickness, volume

of pores, surface area of pores, and cumulative pore volume and pore surface area is given in Table II. In the file named FILERP are the 40 incremental pressure steps commencing from at relative pressure of 0.86 down to 0.08 in steps of 0.02 (Table I). The values of the Kelvin radius were calculated from the Kelvin equation (equation 2) Table IV). The statistical thickness of the adsorbed layers on the solid, as a function of relative pressure was calculated from the experimental plot of the data used by Shull (20).

3. RESULTS

3.1 Density of Compacts

From the final weight, thickness and diameter of each compact the compact density was calculated for every different compaction force and powder (Table III). Figure I shows that the increase in compact density of magnesium oxide reaches a maximum at a compaction pressure of 280 MPa, while for bentonite and magnesium trisilicate the compact densities were still increasing at the maximum compaction pressure used.

3.2 Nitrogen Adsorption

3.2.1 Uncompacted powders

Analysis of the nitrogen adsorption isotherms in the relative pressure range 0.05-0.35 gave, from the B.E.T. equation, mean surface area of 13.1 m^2g^{-1} for magnesium oxide, 32.5 m^2g^{-1} for bentonite and 360.0 m^2g^{-1} for magnesium trisilicate. The surface areas obtained from the B.J.H. computer model were 13.4,32.3, and 203 m^2g^{-1} for magnesium oxide, bentonite and magnesium trisilicate respectively.

A typical computer readout is given in Table I. The calculation shown is for magnesium trisilicate

TABLE 1

PORE MODEL OF BARRETT, JOYNER AND HALENDA

CYLINDRICAL PORES

Relative Pressure	Volume Adsorbed 3 cc/gm	Kelvin Radius A	Stat Layer A	Pore Radius A	Vol Pore Group 3 cc/gm	Area Pore Group 2 M-GM	Cum Area 2 M/GM
0.8600	107.000	61.84	11.23	73.1			
0.8400	104.800	53.50	10.70	64.2	0.0048	1.4	1.41
0.8200	102.900	47.00	10.25	57.2	0.0042	1.4	2.81
0.8000	101.100	41.80	9.86	51.7	0.0041	1.5	4.31
0.7800	99.600	37.54	9.51	47.1	0.0034	1.4	5.70
0.7600	98.100	33.99	9.20	43.2	0.0035	1.5	7.25
0.7400	96.700	30.98	8.92	39.9	0.0033	1.6	8.84
0.7200	95.500	28.39	8.67	37.1	0.0028	1.5	10.31
0.7000	94.400	26.15	9.43	34.6	0.0026	1.5	11.78
0.6800	93.400	24.18	8.22	32.4	0.0024	1.4	13.22
0.6600	92.300	22.45	8.01	30.5	0.0027	1.7	14.96
0.6400	91.500	20.90	7.83	28.7	0.0019	1.3	16.26
0.6200	90.800	19.51	7.65	27.2	0.0017	1.2	17.45
0.6000	90.000	18.26	7.48	25.7	0.0021	1.5	18.97
0.5800	89.400	17.12	7.32	24.4	0.0014	1.1	20.11
0.5600	88.800	16.09	7.17	23.3	0.0015	1.2	21.33
0.5400	87.700	15.14	7.03	22.2	0.0031	2.8	24.10
0.5200	87.500	14.26	6.89	21.2	0.0001	0.1	24.23
0.5000	87.000	13.46	6.76	20.2	0.0012	1.2	25.40
0.4800	86.500	12.71	6.63	19.3	0.0012	1.3	26.65
0.4600	86.000	12.01	6.51	18.5	0.0013	1.3	27.99
0.4400	85.400	11.36	6.39	17.7	0.0017	1.8	29.82
0.4200	85.000	10.75	6.27	17.0	0.0009	1.1	30.88
0.4000	84.000	10.18	6.16	16.3	0.0017	2.1	32.96
0.3800	83.900	9.64	6.05	15.7	0.0014	1.7	34.65
0.3600	83.400	9.13	5.94	15.1	0.0014	1.8	36.44
0.3400	82.900	8.65	5.83	14.5	0.0014	1.9	38.33
0.3200	82.500	8.19	5.73	13.9	0.0010	1.4	39.70
0.3000	82.000	7.75	5.62	13.4	0.0014	2.1	41.81
0.2800	81.500	7.33	5.52	12.8	0.0015	2.2	44.03
0.2600	81.000	6.92	5.42	12.3	0.0015	2.3	46.35
0.2400	80.500	6.54	5.31	11.8	0.0015	2.4	48.77
0.2200	80.000	6.16	5.21	11.4	0.0015	2.5	51.29
0.2000	79.300	5.80	5.11	10.9	0.0025	4.5	55.82
0.1800	78.600	5.44	5.00	10.4	0.0025	4.7	60.50
0.1600	77.800	5.09	4.89	10.0	0.0024	4.9	71.34
0.1200	76.200	4.40	4.66	9.1	0.0035	7.6	78.94
0.1000	75.000	4.05	4.53	8.6	0.0053	12.1	91.01
0.0800	73.800	3.69	4.39	8.1	0.0050	12.1	103.09
					0.0905		

TABLE 2

FORTRAN PROGRAMME FOR B. J. H. EQUATION

The authors will supply this program on request

TABLE 3

COMPACT DENSITIES FOR MAGNESIUM OXIDE BENTONITE AND MAGNESIUM TRISILICATE

Uncompacted Powder	Density ($kg\ m^{-3} \times 10^3$)		
	Mag. Oxide 3.05	Bentonite 2.71	Mag. Trisilicate 2.20
Compressive Force (MPa)			
17.5	-	-	0.86
34.9	1.416	1.784	-
70.0	1.549	1.931	1.006
140.3	1.770	2.052	1.139
161.3	-	-	1.160
174.2	-	-	1.188
210.4	1.805	2.129	1.200
280.6	1.903	-	1.460
350.7	1.817	-	-
430.9	1.816	-	-
490.6	1.817	-	-

compacted at 210.4 MPa, but the calculation of the pore size distribution and intraparticle porosity is also applicable to uncompacted powders. Columns 1 and 2 contain the 40 selected experimental values of relative

TABLE 4

Brunauer Emmett and Teller (B.E.T.) equation:

$$\frac{P}{P_o - P} \quad \frac{1}{V_a} = \frac{1}{V_m C} + \frac{C-1}{V_m C} \quad \frac{P}{P_o} \qquad (1)$$

Kelvin equation:

$$\ln \frac{P}{P_o} = \frac{2\,\delta V}{r_k R T} \qquad (2)$$

where P/P_o = relative pressure (P and P_o are experimental and saturated vapour pressure respectively)

V_a and V_m = experimental and monolayer volume of nitrogen adsorbed

C = adsorption constant. surface tension of adsorbate.

Barrett, Joyner and Halenda (B.J.H.) equation:

$$V_{pn} = R_n \Delta V_n - R_n C \Delta t \sum_{J=1}^{n-1} A_{pJ} \qquad (3)$$

where V_{pn} and ΔV_n = the pore volume at the nth incremental stage and the measurable volume of desorbed gas respectively

Δt_n = thickness of adsorbed gaseous layer between two incremental steps

A_{pJ} = area of pores after J incremental stages

R_n = $r_p^2 / (r_k + t)^2$ a function to accelerate computer computation

C = ratio of average pore radius between two incremental steps to the average pore radius calculated from the upper relative pressure desorption step

= $(\bar{r}_p - t)/ \bar{r}_p$

r_p and r_k = pore and Kelvin pore radius, bar values are mean values

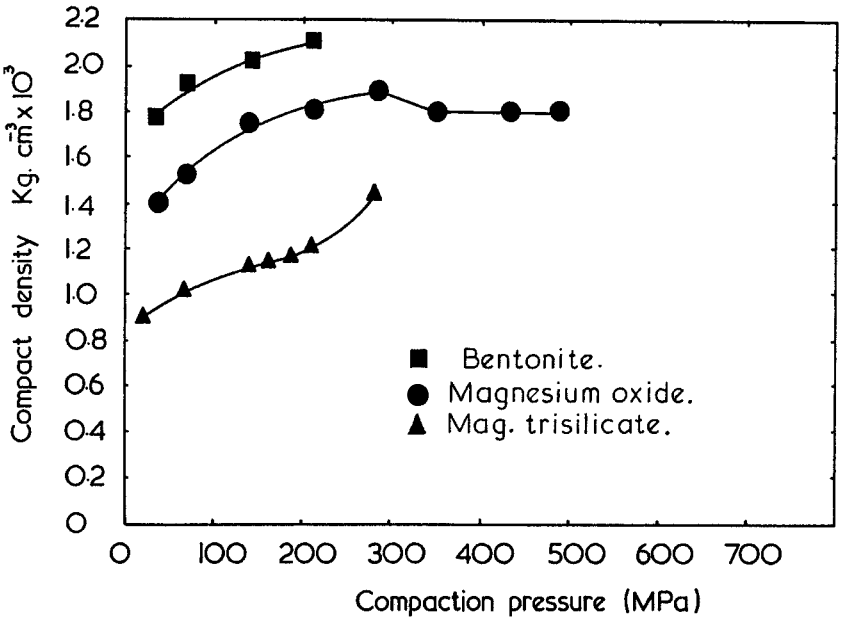

Fig. 1 Compact density of magnesium oxide, bentonite and magnesium trisilicate versus compaction pressure.

pressure and volume adsorbed onto the surface of one gram of powder or compact.

Columns 3 and 4 contain the numerical values, in Angstroms, from the calculation of Kelvin's radius and the statistical thickness of the adsorbed nitrogen layer at specific relative pressures. Column 5 is the pore radius, in Angstroms, which is obtained by the horizontal summation of columns 3 and 4 ($r_p = r_k + t$).

Column 6 is the volume of all the pores within a specific group of pores. Each pore group is evaluated from and limited to the magnitude of the relative pressure incremental step, and thus the size range of the pore group, can be varied to suit the degree of resolution of pore sizes required.

The summation at the bottom of column 6 is the total volume of all measured pores within the porous solid and is termed the intra-particle porosity. The penaltimate column is the contribution that each specific sized group of pores makes to the total surface area of the solid. The final column (column 8) is the cumulative surface area (S_{cum}) from all the pore groups.

A plot of pore radius (column 5) versus volume per pore group (column 6) or area per pore group (column 7) gives the volume-pore size or area-pore size distribution respectively.

3.2.2 Compacted powders

The nitrogen adsorption isotherms obtained over the relative pressure range 0.08-0.86 were computer analysed to calculate the surface areas and intrapar-particle porosities of the particles within the compacts. Table 5 shows the surface area determined by the B.E.T. equation (S_{BET}) and the cumulative pore volume surface area (S_{cum}) determined by the B.J.H. equation. The variation of the B.E.T. surface area with degree of compaction is shown in figure 2. The maximum radius of the group of pores measured by nitrogen adsorption in the three porous materials at the relative pressure of 0.84 is 64.2 Å (6.42 nm). The minimum radius of pore measured by this technique, at a relative pressure of 0.08 to 8.1 Å (0.81 nm).

The interparticle voidage within compacts was obtained by the subtraction, from the reciprocal of the compact density, the reciprocal of the solid density and the intraparticle porosity of the particles within the appropriate compact. Table 6 shows the calculated interparticle voidage for compacts of magnesium oxide, bentonite and magnesium trisilicate with the degree of compaction.

TABLE 5

SURFACE AREA AND INTRAPARTICLE POROSITIES OF MAGNESIUM OXIDE, BENTONITE AND MAGNESIUM TRISILICATE

	Magnesium Oxide			Bentonite			Magnesium Trisilicate		
	Surface Area $m^2\ g^{-1}$		Intra-particle Porosity $cm^3\ g^{-1}$	Surface Area $m^2\ g^{-1}$		Intra-particle Porosity $cm^3\ g^{-1}$	Surface Area $m^2\ g^{-1}$		Intra-particle Porosity $cm^3\ g^{-1}$
	(S_{BET})	(S_{CUM})		(S_{BET})	(S_{CUM})		(S_{BET})	(S_{CUM})	
Uncompacted Powder	13.1	13.4	0.0136	32.5	32.2	0.0315	360	202	0.116
Compressive Force (MPa) 17.5							291		0.103
34.9	12.4	16.1	0.0165	18.1	21.8	0.0256			
70.0	12.6	15.9	0.0230	17.3	22.8	0.0265	320	115.4	0.112
140.3	11.9	15.2	0.0211	18.0	23.1	0.0262	294	114.0	0.097
161.3							213	97.6	0.093
174.2							208	103.1	0.089
210.4	10.9	16.6	0.0192	18.6	23.8	0.0273	213		0.081
280.6	10.9	16.6	0.0169						
350.7	11.1	14.8	0.0137						
430.9	11.2	20.9	0.0362						
490.6	12.3	16.0	0.0171						

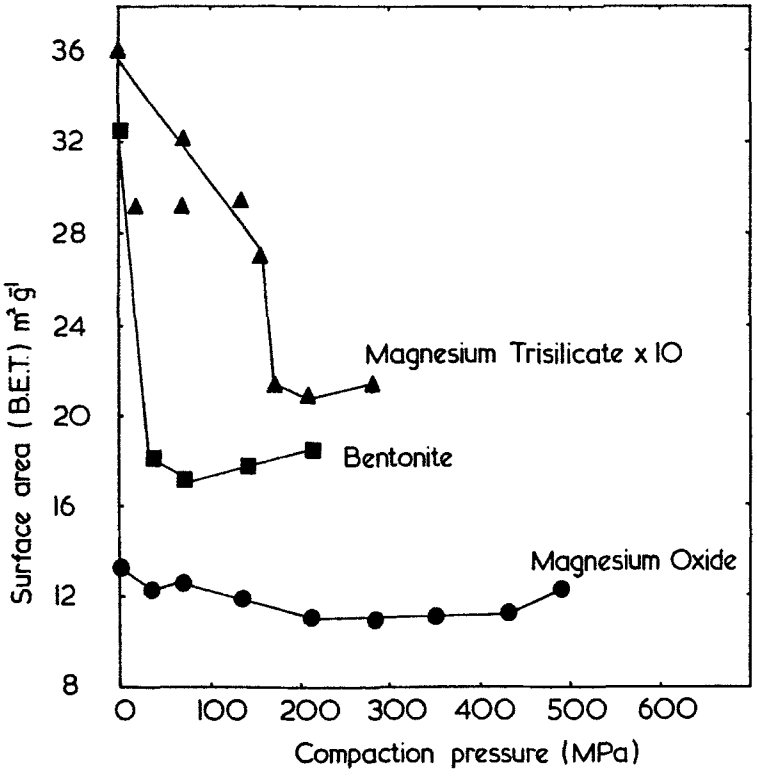

Fig. 2 Variation of B.E.T. surface area with compaction pressure.

The variation of both intraparticle porosity and interparticle voidage as a function of compaction pressure for all three powders is shown in figures 3 and 4.

3.2.3 Contact area

In an uncompacted powder although there is a small amount of particle-particle contact the method of nitrogen adsorption measures the available surface area of a collection of the discrete individual particles. When subjected to a compaction force the particle-particle contact is usually greater and acts as a cohesive bridge to produce a stable compact. The contact area between some

TABLE 6

INTRAPARTICLE POROSITY, INTERPARTICLE VOIDAGE AND CONTACT AREA FOR MAGNESIUM OXIDE, BENTONITE AND MAGNESIUM TRISILICATE

Powder	Compaction Pressure MPa	Intra-Porosity cm^3g^{-1}	Inter-Voidage cm^3g^{-1}	Contact Area m^2g^{-1}
Magnesium Oxide	0.0	0.0136		
	34.9	0.0165	0.357	0.35
	70.0	0.0230	0.291	0.25
	140.3	0.0211	0.212	0.60
	210.4	0.0192	0.203	1.10
	280.6	0.0169	0.176	1.10
	350.7	0.0137	0.204	1.00
	430.9	0.0362	0.183	0.95
	490.6	0.0171	0.201	0.40
Bentonite	0.0	0.0315		
	34.9	0.0256	0.165	7.60
	70.0	0.0265	0.123	7.20
	140.3	0.0262	0.092	7.15
	210.4	0.0273	0.073	6.95
Magnesium Trisilicate	0.0	0.116		
	17.5	0.103	0.607	34.5
	70.0	0.112	0.427	35.0
	140.3	0.097	0.326	33.0
	161.3	0.091	0.321	45.0
	174.9	0.093	0.294	76.5
	210.4	0.089	0.266	76.0
	280.6	0.081	0.149	73.5

types of material increases with increase in compaction pressure and therefore reduces the available compact surface area. A simple approach in the measurement of con-

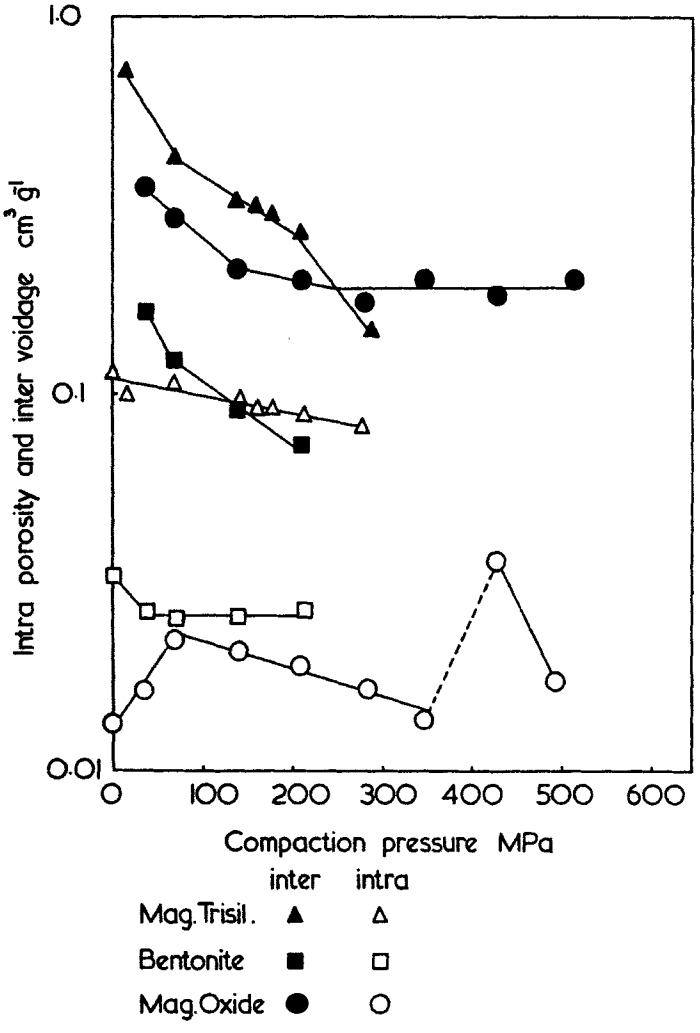

Fig. 3 Intraparticle porosity and interparticle voidage variation with compaction pressure.

tact area is to take half the difference between the surface area before and after compaction.

Calculation of the contact areas by this method for magnesium oxide bentonite and magnesium trisilicate are

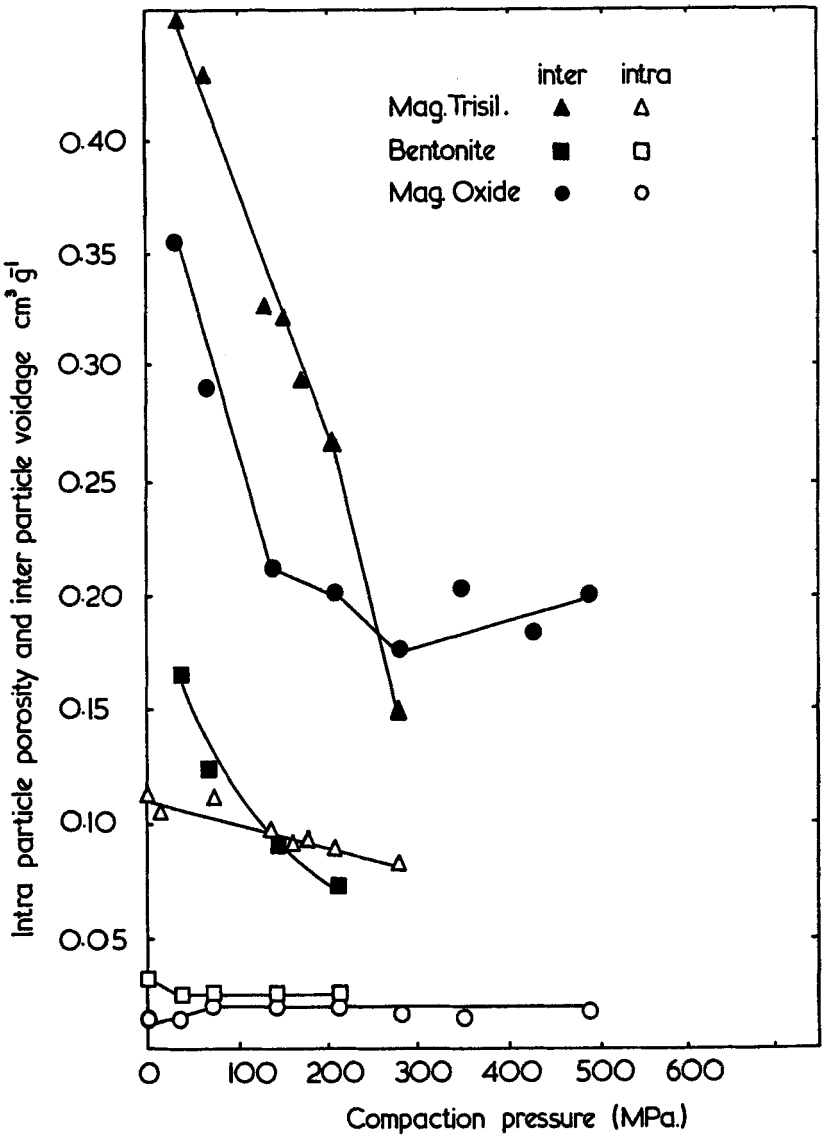

Fig. 4 Logarithmic variation of particle porosity and compact voidage with compaction pressure.

given in Table 6. A graph of the variation of particle-particle contact area with degree of compaction is shown in figure 5.

4. DISCUSSION

4.1 Magnesium Oxide Compacts

The overall trend for all powders investigated is, as expected, an increase in densification as the compaction pressures above 350 MPa shows a constant compact density which normally would indicate that the particles of powder have been bonded together to give an optimum densification. From calculation of the intraparticle porosity and the interparticle voidage (figures 3 and 4) it can be seen that the interparticle voidage, within magnesium oxide compacts, produced in the range 150-425 MPa, changes very little. It is the deformation of the porous particles and the decrease in particle porosity which accounts for the increase in compact density. Knowledge of the change that occurs within the compact is only possible from the measurement of the nitrogen adsorption and molecular nitrogen penetration into the internal structure of the compact and could not be obtained from the bulk dimension of the compact (figure 1).

In the initial stages of magnesium oxide compaction, up to a compaction pressure of 70 MPa, the intraparticle porosity increases while the interparticle voidage decreases. The phenomena of intraparticle increase can be explained only by the assumption that magnesium oxide particle fracture under pressure and expose enclosed pores, which, when measured by nitrogen adsorption, increase the particle porosity. At compaction pressures greater than 70 MPa the intraparticle porosity then decreases from a maximum of 0.023 $cm^3 g^{-1}$. The decrease in intraparticle porosity menas that either no further size reduction occurs in the porous magnesium oxide particles and the

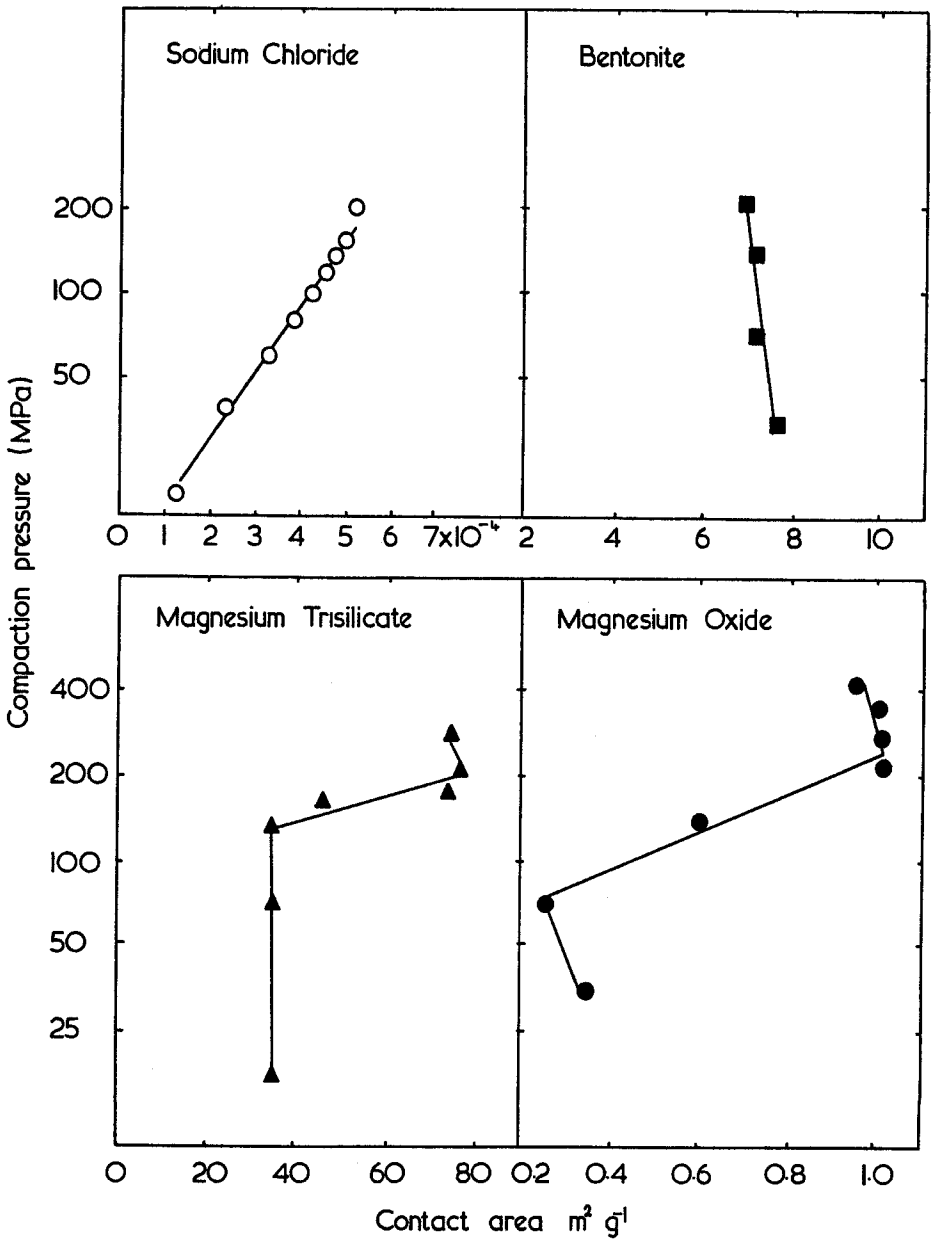

Fig. 5 The effect of compaction pressure on particle-particle contact area.

pores are reduced in size by the compaction pressure or that fragments of magnesium oxide so produced are so small that the fragments contain a smaller and smaller range of pore sizes. Since the pore size range in uncompacted magnesium oxide is between 1.8-12.0 nanometer diameter, it was assumed that no further size reduction occurred above a compaction pressure of 70 MPa as it is likely that the particle size of the magnesium oxide fragments would be in the nanometer range. The subsequent intraparticle porosity decrease in the range of 70-350 MPa must therefore be due to the internal deformation of the magnesium oxide particle.

The interparticle voidage decreases down to an approximate value of 0.20 $cm^3\ g^{-1}$ at a compaction pressure of 150 MPa and then remains relatively constant up to a pressure of 430 MPa. The small change in the interparticle voidage and the larger decrease in the intraparticle porosity in this compaction pressure range suggests that magnesium oxide particles could be regarded as a soft malleable material which has angularly shaped particles. The angular nature of the particles, or its fragments, prevents the movement of particles and thus a decrease in voidage.

4.2 Bentonite Compacts

With bentonite the intraparticle porosity of the particles within the compacts remains constant between the compaction pressure range 35.0-210 MPa, the interparticle voidage however steadily decreases with compaction pressure. The non-increase of intraparticle porosity of bentonite particles with compaction pressure indicates that no internal structural deformation occurs, nor is there any exposure of enclosed pores by particle fragmentation. The assumption that non-fragmentation of particles occur is valid because of the decrease in B.E.T.

surface area (figure 2) seen on compaction of the loose powder. The steady decrease in interparticle porosity is similar to that seen with magnesium oxide compacts in the pressure range 35-140 MPa. The mechanism of compaction of bentonite and magnesium oxide will however be different because there is no fragmentation of the gentonite particles.

4.3 Magnesium Trisilicate Compacts

With magnesium trisilicate both the intraparticle porosity and the interparticle voidage decrease logarithmically with compaction pressure over the range 18.0-280 MPa. The interparticle voidage of magnesium trisilicate porosity (figures 3 and 4). The reduction of B.E.T. surface area (figure 2) and also the reduction of the intraparticle porosity with compaction pressure shows that no fresh surface is exposed due to the fracture of particles.

4.4 Contact Area of Compacts

An insight into the mechanism of compaction can be obtained from the knowledge of the contact area of the particle-particle bond and the variation of surface area, intraparticle porosity and interparticle voidage with compaction pressure. The degree of contact area which exists between a particle-particle bond at different compaction pressures for magnesium oxide, magnesium trisillicate, bentonite and sodium chloride is shown in figure 5. The contact area of the plastic deforming material, sodium chloride, at different compaction pressures was calculated from the data of Hardman and Lilley.

Magnesium trisilicate shows little change in contact area over the compaction pressure range 18.0-140 MPa. The change in B.E.T. surface area (figure 2) must however be reconciled with the large change in the interparticle voidage of magnesium trisilicate over this pressure range. The mechanism of compaction is therefore due to particle

rearrangement and not to the formation of particle-particle bond which would have produced a measurable contact area. Above a compaction pressure of 140 MPa the contact area rapidly increases up to a pressure limit of 180 MPa. At this pressure deformation of magnesium trisilicate particles occur as seen from the compact density curve (figure 1) and the interparticle voidage curve (figures 3 and 4). The slope of the contact area versus compaction pressure for magnesium trisilicate between the pressure range 140-280 MPa is similar to that of sodium chloride which is known to deform and produce a particle-particle bond by plastic deformation. It can thus be surmised that magnesium trisilicate in the pressure range 140-280 MPa produces a similar plastic particle-particle bond.

The interparticle voidage versus B.E.T. surface area curve (figure 6) for magnesium trisilicate between 18.0-140 MPa shows that although the interparticle voidage changed considerably, the surface area of the compact was approximately constant.

Since the compaction pressure on the powder did not create or destroy the surface area of the uncompacted powder, the particles have to undergo a particle rearrangement to obtain densification of the powder.

In the range 140-174 MPa the surface area of compacts of magnesium trisilicate decreased rapidly until above a pressure of 170 MPa very little change occurred. The region of rapid surface area decrease corresponds to the region of plastic deformation seen in figure 5.

Although the compacts of magnesium oxide produced at 34.9 and 70.0 MPa also showed little change in contact area (figure 5), the mechanism of compaction at these pressures is unlikely to be similar to that of magnesium trisilicate particle rearrangement. The mag-

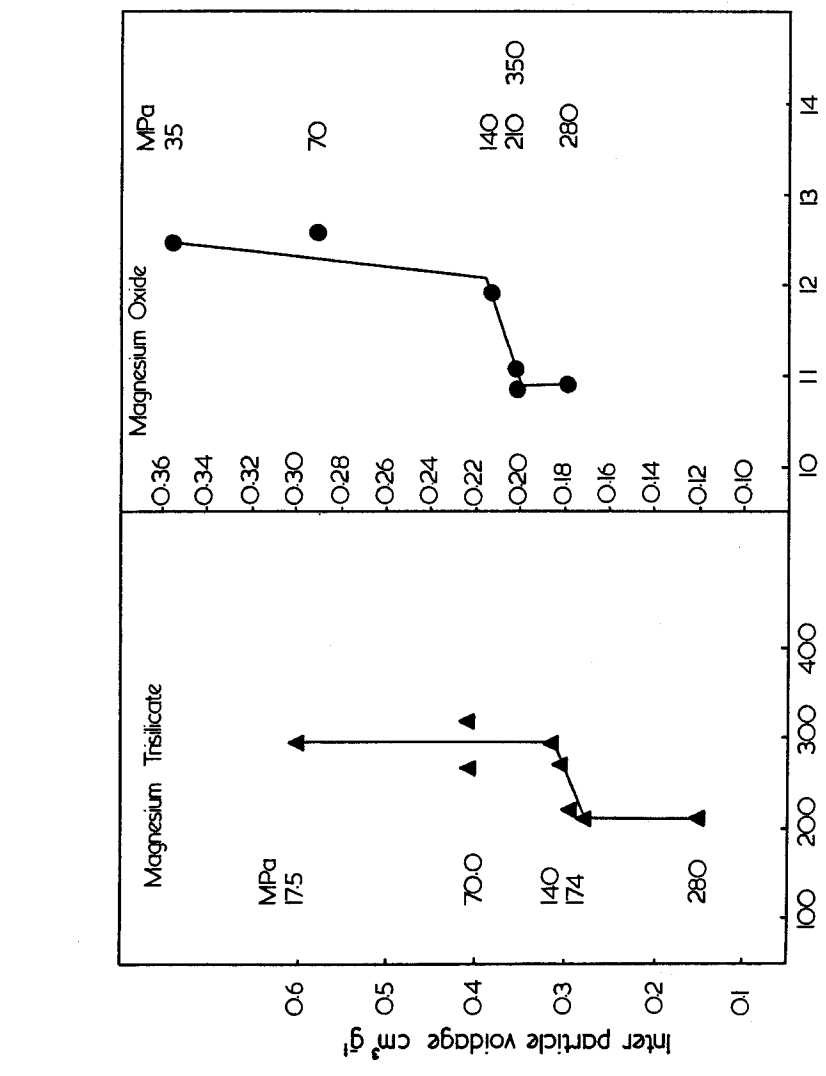

Fig. 6 Variation of interparticle voidage with the B.E.T. surface area of compacts.

nesium oxide particle rearrangement will be due to fracture fragments of magnesium oxide moving away from the load bearing areas into the interparticle spaces. The existence of these magnesium oxide fracture fragments is possible because the B.E.T. surface area only showed slight decrease in compact surface area at low compaction pressure, unlike the rapid decrease seen with magnesium trisilicate and bentonite in the same pressure range. The variation of contact area of magnesium oxide with compaction pressure in the region 70-280 MPa is similar to that of magnesium trisilicate and sodium chloride, but a reduction in contact area occurs with compacts produced at compaction pressures greater than 280 MPa. The whole region of the magnesium oxide contact area-pressure profile is however badly defined which is possibly due to the ease with which particles of magnesium oxide begin to fracture.

Magnesium oxide shows a similar interparticle voidage versus B.E.T. surface area profile to that of magnesium trisilicate (figure 6). The reduction in surface area, in the compaction pressure range 140-350 MPa is less with magnesium oxide than with magnesium trisilicate.

The contact area-pressure curve for bentonite shows no plastic contact region similar to sodium chloride and magnesium trisilicate and only a small change in the compact B.E.T. surface area and intraparticle porosity at different compaction pressures. The increase in densification (figure 1) is therefore not due to plastic particle-particle contact.

5. CONCLUSION

Knowledge of the surface area of compacted and uncompacted powders plus the calculation of intraparticle porosities of particles within compacts and the inter-

particle voidage of compacts from adsorption isotherms can give an insight into the mechanisms of compaction. The evaluation of the contact area, between particle and particle, produced at various compaction pressure can show whether the bond is achieved by plastic deformation or particle rearrangement.

REFERENCES

1. Armstrong, N.A. and Haines-Nutt, R.F., Proc. 1st Int. Conf. on Comp. and Consolid. of Part. Matter, Brighton, October 1972, Powder Advisory Centre.

2. Bal'shin, M. Yu., Dokl Akad Hank SSSr, 67, 831 (1949).

3. Barrett, E.P., Joyner, L.G. and Halenda, P.P., J. Am. Chem. Soc., 73, 373 (1951).

4. British Standard 4359: Part 1: 1969, British Standards Institution, 2 Park St., London, W1.

5. Brunauer, S., Emmett, P. H. and Teller, E., J. Amer. Chem. Soc., 60, 309 (1938).

6. Cranston, R. W. and Inkley, F. A., Advances in Catalysis, 9, 143 (1957).

7. Fuhrer, C. and Ghadially, J., Acta Pharm. Suec., 3, 201 (1966).

8. Goetlel, C.G., Treatise on Powder Metallurgy Interscience, New York, 1949.

9. Hardman, J.S. and Lilley, B.A., Proc. Roy. Soc. Lond., A333, 183 (1973).

10. Heckel, R.W., Trans. Am. Inst. Min. Metall. Engrs., 221, 671 (1961).

11. Higuchi, T., J. Am. Pharm. Ass., XLIII, 685 (1954).

12. Higuchi, T., Elowe, L.N. and Busse, L.W., J. Amer. Pharm. Ass., (Sci. Ed.), 43, 685 (1954).

13. Innes, W. B., Analytical Chemistry, 29, 1069 (1957).

14. Kawakita, K. and Lüdde, K. H., Powder Technology, 4, 61 (1971).

15. Newitt, D. M. and Conway-Jones, J. M., Trans. Instn. Chem. Engrs., 36, 422 (1958).

16. Pierce, C., J. Phy. Chem., 57, 149 (1953).

17. Roberts, B. F., J. of Colloid and Interface Sci., 23, 266 (1967).

18. Rumpf, H., Chem. Ing. Tech., 1958, 30, 144 (1958).

19. Shapiro, I., Technical Report No. ASD-TDR-63-147. Directorate of Mat. and Process, Wright-Patterson Air Force Base, Ohio, USA, March 1963.

20. Shull, C. G., J. Am. Chem. Soc., 70, 1405 (1948).

21. Train, D., J. Pharm. Pharmacol., 8, 745 (1956).